

# A Multispectral Ariel Image Stitching using Decortification and EEG Signal Extraction Technique

Mukul Manohar S<sup>1</sup>, Dr. K N Muralidhara<sup>2</sup>

Assistant Professor<sup>1</sup>, Professor<sup>2</sup>

Department of Electronics & Communication Engineering-Vemana Institute of Technology  
(Affiliated to VTU, Belagum), Bengaluru, India<sup>1</sup>

Department of Electronics & Communication Engineering-PES College of Engineering, Mandya, India<sup>2</sup>

**Abstract**—UAV Videos and other remote-sensing innovations have increased the demand for multispectral image stitching methods, which can gather data on a broad area by looking at different aspects of the same scene. For large-scale hyperspectral remote-sensing images, state-of-the-art techniques frequently have accumulating errors and high processing costs. However, this research paper aims to produce high-precision multispectral mapping with minimal spatial and spectral distortion. The stitching framework was created in the following manner: First, UAV collects the raw input data, which is then labeled as a signal using a connected component labeling strategy that correlates to each pixel or label using the EEG (Alpha, Beta, Theta, and Delta) technique. Next, the feature extraction process follows a novel decortification Hydrolysis CNN approach which extracts active and passive characteristics. Then after feature extraction, a novel chromatographic classification approach is employed for separating features without overfitting. Finally, a novel yield mapping georeferencing technique is employed for all images stitched together with proper alignment and segmented overlapping fields of view. The suggested deep learning model is an effective method for real-time mosaic image feature extraction which is faster by an average of 11.5 times compared to existing approaches as noted on the samples for experimental analysis.

**Keywords**—EEG signal extraction; feature extraction; image stitching; multispectral image; UAV video

## I. INTRODUCTION

Unmanned Aerial Vehicles (UAVs) fascinated a whole lot of people in many nations as soon as they were developed and have since been widely used in both the military and civilian sectors (such as for mapping, catastrophe monitoring, and crowd monitoring) as well as for in-flight investigation and border patrol. The photographs captured by UAVs have several undesired qualities, like big numbers, short image vicinity, a partly cover degree, and multiple strips, due to the restrictions of flying height and camera focal length. It is crucial to achieve a complete panoramic perspective using quick image fusion techniques to gain more detailed information and broaden the range of vision in many particular tasks [1]. The usage of image fusion technology, which has become a hot research area, is common in multimedia applications including virtual reality, remote sensing image processing, and video surveillance where the watching component has a tiny field of view but the expected observation is large. Users have access to a variety of software applications, like Autopano and Panorama Photo Stitcher, in the market for creating panoramas.

According to the registration strategy, there are four broad groups for picture mosaic techniques [2]. The first technique relies on the intensity levels or colors of each pixel; while this scheme is straightforward, it performs poorly in terms of noise avoidance and blending effectiveness. The second technique relies on the transform features, which has high noise resistivity, but the stitching requires a lot of calculations and the results are subpar when the image changes in view perspective or zoom. The other technique is based on features, for which the stitching efficiency, resilience, and accuracy of the algorithms are often high and they are typically similar to image size editing, transformation, and rotation. The three conventional feature extraction algorithms are Harris, Scale-Invariant Feature Transform [3], and Oriented Fast and Rotated Brief. On deep learning, the final one is based. Many deep learning methods based on feature extraction and matching have been created to perform picture registration [4]. Despite the recent advancements in image mosaic technology, several techniques still fall short of the instantaneous, reliable, and accuracy demands of UAV image fusions. UAV pictures have a lot of data, tiny phase amplitude, and a higher degree of overlapping [5], among other qualities. Since a UAV video/image contains a lot of data, the mosaic process takes an unacceptably long time [6]. Second, because they are frequently small, UAVs struggle to maintain themselves and are poorly wind-resistant. There will unavoidably be some tilting when taking pictures, even though they have an autopilot and a stabilizing gyroscope. Images captured by UAVs contain significant affine distortion in comparison to the actual scene due to the geometric distortion of the camera caused by the lens [7]. To address this problem, researchers have proposed mounting high-resolution cameras on a UAV. The dimensional fault, which is the difference between the relative offset and the absolute offset, can be thought of as low-frequency noise brought on by the UAV drift, and it can be addressed by using a high-pass filter [8].

The projection matrix-based approach can also be used to extract supreme structural offset from the drone footage, presuming that out-of-plane offsets can be disregarded. The projection matrix was determined using stationary backdrop features, and then it was further honed using the constrained bundle adjustment optimization approach to reduce the re-projection error. Additionally, for this technique to work, the camera must move rather quickly; otherwise, the camera settings in successive frames would be very much close, which will cause a major inaccuracy when applying the bundle

adjustment. However, in-field measurements, the expanse between immobile locale objects and the drone is typically many times greater than the drone motion itself, thus making this approach inapplicable. With the help of homography, also referred to as perspective transformation, it is possible to adjust the camera movement for a planar outlook without the use of camera constraints [9].

Although the homography related methods are numerically effective, there are numerous obstacles in the way of its straight-forward application to the counting of dynamic offsets of massive structures. Because of the limited pixel resolution, it's possible that the camera won't be able to sufficiently capture both the offset measurement points and immobile areas of the organization (i.e., the homography characteristics) in a single image. However, choosing at random from these areas could cause big inaccuracies in the homography computation result. The chosen homography characteristics is expected to be over or near the flat surface in which structural motion occurs since homography requires a planar scene and not all random homographies are realistic picture alterations [10]. And the system's created aerial panorama could have poor aesthetic flaws at pivot points. Then, the stitching is successful for neighboring frames in image sequences where the stitching has been successful in order, but it can be challenging to guarantee the overall stitching effect in multistrip long-distance trips [11]. Additionally, it is challenging to produce useful data from sequences gathered by UAVs during multistrip missions and it is laborious to manually track the chosen homography elements in each frame of a video. The stitching effect, however, can be diminished with a greater volume of images and much identical parts in the prospect [12]. However, it is difficult finding a stationary landmark during an earthquake.

In this work proposed, a novel live drone image mosaic system is proposed. The main contributions are as follows:

- First, proposed a state-of-the-art, real-time framework for drone image mosaicking. The architecture comprises automatic initialization, feature extraction & classification, and live mosaic generation. The setup procedure uses EEG to automatically identify the image clips based on brainwaves (Alpha, Beta, Theta, and Delta).
- After that, all four of these brainwaves are subjected to a feature extraction procedure utilizing deep learning, where a mixture of alpha and beta is used to examine active features while theta and delta are used to consider passive features.
- After feature extraction, the classification process is done then finally real-time mosaic creation makes up the framework's entire structure.
- The primary tasks required in the controlling of large areas, including mosaicking, feature extraction, and classification, are improved in accuracy compared to existing drone-based techniques.

The remaining portion of the paper is structured as follows: Section II explains briefly the existing literature and the research gaps. Section III gives an overview of the proposed

work. Section IV details the proposed system architecture. Section V discusses the results and analysis of implementation. Section VI finally concludes the work.

## II. RELATED STUDY

There has been interesting works available in the literature that paves way for the growth of the techniques and the technology responsible for image applications. Avola et al. [13] proposed the best parameters to automatically predict, specifically, depth and frame rate to recognize the three factors in previous section are suggested and tested. The dimensions of the aimed object to be analyzed, the UAVs' travel speed, and the primary inner dimensions of the video sensor, such as the focal length, field of view, and pixel size, are some of the criteria that are used to estimate the parameters. Both man-made videos produced with the in-flight data and Robotics Simulation (AirSim) and actual film sequences reported in the UAV Mosaicking and Change Detection (UMCD) and NPU Drone-Map datasets served to demonstrate the suggested method's complete effectiveness on the objective. However, ensuring the minimal spatial resolution necessary to complete a given activity is the primary issue to be addressed regarding flying height.

Ranghao et al. [14] proposed a live drone image fusion architecture that solely utilizes the UAV picture frames and does not depend on the global positioning system (GPS), ground control points (CGPs), or any other auxiliary data. Through the use of this framework, it is hoped to produce high-quality panoramas while reducing spatial distortion and speeding up mosaicking operations before choosing key frames to increase efficiency, the framework evaluates the general setting of every new frame to be added. Then, to perform an accurate position computation of the existing scene and lessen the bend brought on by increasing mistakes, a new optimization method based on minimizing weighted reprojection errors is implemented. To produce the best mosaic output, the local picture is fused and updated in real-time using the weighted partition fusion approach based on the Laplacian pyramid. UAVs frequently capture multi-strip and large-scale image sequences, however, it is challenging to create panoramas directly from the stitched photos, and some of the feature points are unstable and challenging to extract.

Srivastva et al. [15] proposed an overview of deep learning methods for on-ground vehicle recognition utilizing aerial data obtained by UAVs (often referred to as drones). To review the works, it is important to consider both the optimization goal and the method used to increase accuracy and decrease computation overhead. To illustrate the parallels and discrepancies between different approaches and to draw attention to the remaining issues in this field, this work is a useful study. Researchers studying AI, traffic surveillance, and UAV applications will find this survey to be useful. However, the processing of a picture takes a long time and results in a lot of false positives.

Woo et al. [16] proposed to drastically lower the error level, identification of fissures was determined using comparative position between components in drone-captured photos rather than using absolute position information. A total of 97 photos were collected using aerial photography. Five

fissures and three reference components were defined using the point-cloud approach, image blending, and homography domain algorithm. Importantly, the comparison of calculated localized values with concrete values obtained from field measurement showed that errors in the range of 24-84 mm and 8-48 mm, respectively, were received based on the coordinates. Additionally, RMSE errors ranging from 37.95 to 91.24 mm were verified. The target concrete construction, however, might not always have enough or the right reference objects accessible.

Rui et al. [17] proposed a Rapid Scale-Invariant Feature Transform (RSIFT) operator to shorten computation time. Then used is the As-Natural-As-Possible (AANAP) technique for picture registration. To remove the motion ghosting, an image segmentation method is used. Finally, a unique collection of aerial photos is created for image mosaics, using which analogous tests using cutting-edge image mosaic techniques are carried out. However, research indicates that SIFT has huge computational complexity.

Zhang et al. [18] proposed an approach based on Oriented Fast and Rotated Brief (ORB) and semantic segmentation. To distinguish between the forefront and surroundings of the image and to get the forefront content, a semantic segmentation network is introduced by the algorithm during image registration. It simultaneously extracts feature points using the quadtree decomposition concept and the conventional ORB approach. The foreground feature points can be removed to achieve feature point matching by comparing the feature point information with the foreground semantic information. The homography domain and the weighted fusion technique will be used to stitch and fuse the images based on precise image registration. However, it is challenging to find trait points in areas with weedy texture, and the major drawback of SIFT is that real-time performance cannot be attained without the aid of hardware or specialized image processors.

In order to locate an intuitively optimal seam in uninterrupted areas of high similarity, Yaun et al. [19] suggested an innovative super pixel-based performance function that incorporates data on material difficulty, color distinction, and gradient difference. Finally, to eliminate seams and provide seamless color transitions, employ an exceptional pixel-based color blending technique. The method is superior to several cutting-edge UAV photo stitching techniques, according to experimental data, and can effectively and rapidly perform seamless stitching. However, owing to the existence of parallax, artifacts always show up in overlapped areas.

Yang et al [20] proposed a straightforward yet effective approach for sewing durable and precise blade images. Introduce the Blade30 dataset, which includes 1,302 real drone-captured photos of 30 entire blades taken in a variety of environments (both on and off-shore) and richly annotated with information on flaws and contaminations, among other things, to encourage further research. By using the recommended patching strategy based on drone-blade lengths and rotor margins at the coarse-grained level, the initial blade portrait is produced. Then, utilizing regression-based roughness and shape losses, fine-grained modifications are optimized. Additionally, this approach makes full use of the drone's

existing knowledge and the characteristics of blade pictures. However, it may be challenging to gather enough labeled data to initiate this, which is primarily due to inefficient inspection techniques.

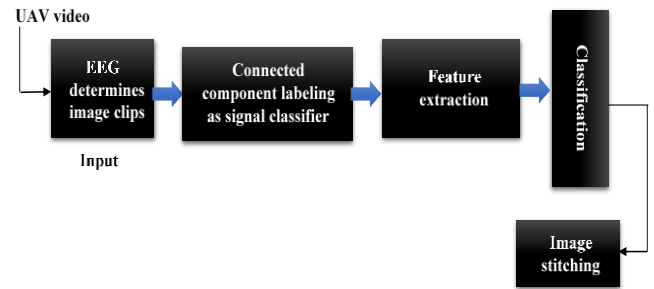


Fig. 1. Block diagram for real-time image stitching of UAV video.

Some of the research gaps identified are: Low-textured picture sewing still presents a number of complicated challenges; since multiple photos were captured from various angles, the patched images also contain projective distortions; Picture stitching combines a number of overlapping images to create a single, larger mosaic with a wider angle of perspective because cameras have a low angle of perspective. Global geometric transformations were typically approximated by older methods for stitching together overlapping pictures; These methods, however, rely on rigid premises that are commonly violated in reality, resulting in defects in the merged images like misalignments or ghosting, such as the camera rotation having a fixed projective center or the scene having a constrained depth variance; Only a small number of points are recognized and matched in some homogeneous regions, making it challenging to predict an exact transformation. The proposed method tries to overcome these challenges and develops an efficient method for image stitching.

### III. OVERVIEW OF THE PROPOSED WORK

The suggested architecture seeks to address the several issues mentioned above for improved target surveillance and real-time image stitching of UAV video. Enhancing real-time target tracks and stitching image serves several purposes, including improved accuracy, easier long-distance stitching, accurate information, and overall performance. It also captures both displacement measurements and homography properties in a single image. UAVs, such as drones or planes, equipped with cameras, sensors, software for control, and interactions, first gather raw data. UAVs can collect visual sensing data via their camera-equipped device. [21]. The pixels or labels in these images are designated as signals, utilizing an analogy to EEG patterns such as alpha, beta, delta, and theta, each linked to distinct frequencies [22]. The process of extracting active and passive features utilizing statistical methodology to ascertain the average weight for all waves and set thresholds is then carried out. If the weighted average value is higher than the threshold, it is considered active else passive. Algorithms based on CNN relate active attributes to alpha and beta, whereas passive attributes are linked to delta and theta. However, this method permits accurate feature extraction,

captures the qualities of both displacement measurement and homography, and has superior accuracy. After this, the classification process follows, effectively segregating these features to prevent overfitting. Finally, using overlapping fields of view, the images are seamlessly combined to provide a segmented, high-resolution image. However, this method makes stitching across large distances simple, provides accurate information, and enhances overall performance. Fig. 1 depicts a block diagram for real-time image stitching of UAV video, which demonstrates raw data. Video is acquired by UAV like a drone or plane, and comprises of a sequence of image clips assessed using EEG. Images are categorized as signals using the connected component labeling technique. Then feature extraction and classification are performed. Finally, the images are seamlessly stitched together to produce a cohesive output.

#### IV. ARCHITECTURE OF THE PROPOSED METHODOLOGY

The proposed design solves low accuracy, overfitting difficulty ensuring stitching effect over long distances, incorrect data, and difficulty capturing both displacement and homography characteristics in a single image. In the beginning, raw data is collected by UAV to capture illustrated sensing information by its camera installed, and the pixels or labels in these images are designated as signals using the connected component labeling technique for using an analogy to EEG patterns such as alpha, beta, delta, and theta, where each linked to distinct frequencies. For removing noise or error in the signal and the signal is then split into two halves using decortification CNN, a proposed feature extraction method that collects both active and passive features. While delta and theta represent passive features, alpha, and beta indicate active features. To identify the alpha, beta, delta, and theta features, use a statistical method. To ensure this, average weights for each wave must be determined, and global thresholds must be set. The characteristic is regarded as active if the estimated weighted average value is higher than the threshold; otherwise, it is regarded as passive.

After feature extraction, classification is carried out by employing the chromatographic approach to separate active and passive features separately without overfitting. However, this approach enables precise feature extraction and categorization and captures both the characteristics of displacement measurement and homography. Finally, a high-resolution image is created by combining all the photographs with their overlapping fields of view, utilizing a yield mapping geo-referenced approach to appropriately align and segment each image. However, this approach makes stitching across vast distances straightforward, high accuracy offers correct data, especially finding stable landmarks after an earthquake is simple and improves overall performance.

The proposed architectural model for the real-time UAV video image stitching process is shown in Fig. 2 which start with the UAV obtaining the raw data and this data comprise a sequence of image clips. Each pixel/label within these images is categorized as a 'signal' using a connected component labeling technique. This idea makes use of the four types of brain waves alpha, beta, theta, and delta to extract active and passive features using CNN, based on their respective

frequencies. The active attributes encompass alpha and beta waves, while the passive attributes encompass theta and delta waves. Subsequently, a classification process utilizing chromatography technique is applied to the extracted features. Finally, the process involves image stitching using a yield mapping geo-referenced technique, seamlessly combining the acquired images.

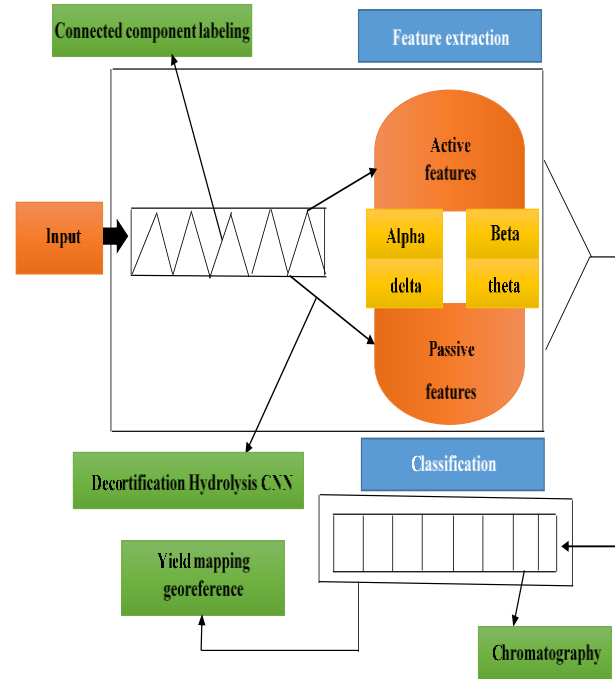


Fig. 2. Proposed architectural model for Real-Time UAV video image stitching.

All of these EEG signal properties (Alpha, Beta, Theta, and Delta) are described below, along with their mathematical expressions:

Average frequency weighting (AFW): The average frequency weighting can be found to estimate the power spectrum of the obtained sequence of signal [22]. Using statistical methods an average value is found for all waves with certain frequency weighting elements. The following mathematical equation can be used to represent the AFW,  $S(k)$  for any  $N$ -point signal  $x(n)$ .

$$S(k) = \frac{1}{N} * W \sum_{K=0}^{N-1} |X_p(k)| \quad (1)$$

where  $n$  is a variable that specifies the data points of the time-domain discrete-time input signal  $x(n)$ . For a total number of temporal data points  $N, 0 \leq n \leq N-1$ . Similar to that,  $k$  also refers to a variable that specifies data points in spectral-domain form  $X_p(k)$  of  $x(n)$ . For a total number of spectral data points  $N, 0 \leq k \leq N-1$  [23].

Repeating this calculation across all frequency bands yields the final Power Spectral Density (PSD) values for Delta, Theta, Alpha, and Beta [24].

The PSD according to Welch is expressed by:

$$P_d(f) = \frac{1}{MU} \left| \sum_{k=0}^{N-1} X_p(k)w(k)e^{-j2\pi fk} \right|^2 \quad (2)$$

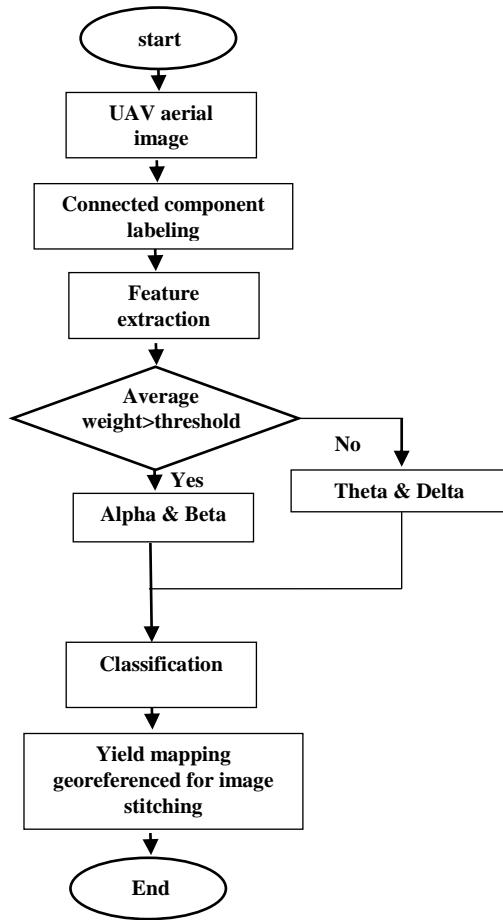


Fig. 3. Flow chart of the proposed architecture.

Let  $x(n)$  be the sequence, with  $N = 1, 2, 3, \dots, N-1$  representing the signal intervals, and  $M$  denoting each interval length.  $U$  is the normalization factor for the power in the window function, and  $w(n)$  is the windowed data, so:

$$U = \frac{1}{M} \sum_{k=0}^{N-1} |w(n)|^2 \quad (3)$$

After extracting all PSD, the alpha, and beta signals are considered active and delta and theta are considered passive features to compare with the overall threshold  $\emptyset$

$$\text{PSD} > \emptyset \text{ or } \text{PSD} < \emptyset \quad (4)$$

The suggested architecture's flowchart is shown in Fig. 3, starting with raw data which is an aerial image that is collected by an UAV as input. A connected component labeling technique is used to classify each pixel or label in these images as a "signal". This concept uses the four different types of brain waves alpha, beta, theta, and delta to extract both active and passive properties. Using a statistical approach, the alpha, beta, delta, and theta features are identified and designated as  $B_1, B_2, B_3, B_4$ , respectively. To do this, average wave weights and global thresholds must be established. The attribute is considered active if the projected weighted average value

exceeds the threshold; otherwise, it is considered passive. The procedure of classification is then performed following feature extraction. Finally segmented using yield mapping georeferenced approach and merged every image with proper alignment.

**Proposed Algorithm:**

Multispectral mapping for image stitching using EEG signal to extract robust feature extraction

**Require:** Multispectral images  $I_p = 1, 2, 3 \dots N$

**Ensure:** Multispectral mapping with high alignment accuracy

**Step 1:** Start  $I_p = 1, 2, 3 \dots N$

**Step 2:** Each pixel in the image is labeled as a signal.

**Step 3:**  $i=1$

**Step 4:** for each sample,  $S_m$  do

**Step 5:** Calculate the average weighted probability for each wave  $B_1, B_2, B_3, B_4$ , and set the threshold  $\emptyset$ .

**Step 6:** Compare weighted probability with threshold

**Step 7:** if  $B > \emptyset$  or  $B < \emptyset$  then

```

{
incorporate  $B_1, B_2$ ;
else {
incorporate  $B_3, B_4$ ;
}
}
i++
end for
    
```

V. RESULT AND DISCUSSION

This section presents the detailed results of the proposed model. To provide a comprehensive performance evaluation, the suggested model was compared to two other models, the SIFT [25] and BRISK [26]. The work was implemented in Python 3.11.4 and the packages used are cv2 and math. Two sample images were used to test the performance of the proposed work.

Fig. 4 shows the input sample 1 image pairs to be stitched. During feature extraction using SIFT algorithm, 4369 features from the first image and 4333 features from the second image are selected as shown in Fig. 5(a) using SIFT. Fig. 5(b) shows the 10038 features and 10774 features selected from images 1 and 2 respectively using BRISK algorithm. Fig 5(c) shows the 500 features from Image 1 and 500 features from image 2 selected using the proposed approach. Fig 6(a), (b) and (c) shows the matching features between the pairs of images using SIFT, BRISK and the proposed algorithm respectively. Fig. 7 shows the sample 1 image pairs fused.

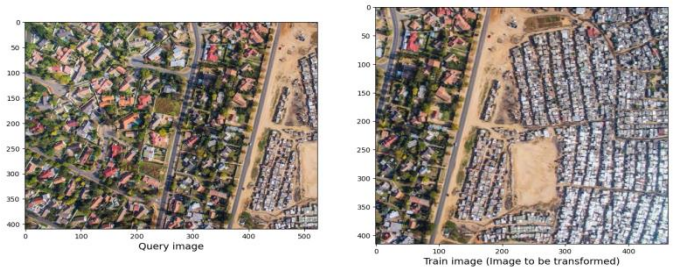
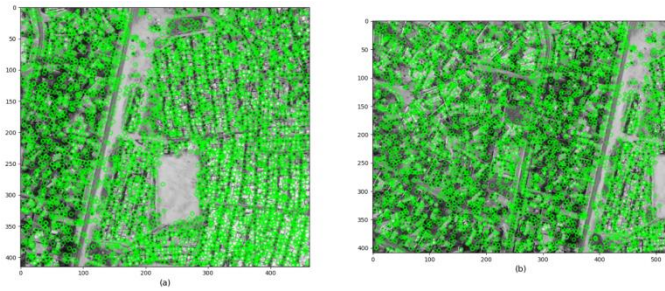
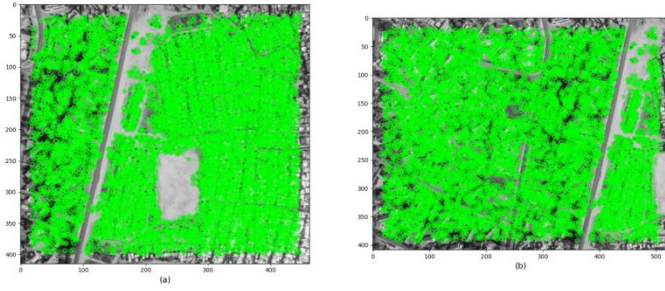


Fig. 4. Input Sample 1: Image1 and Image2.



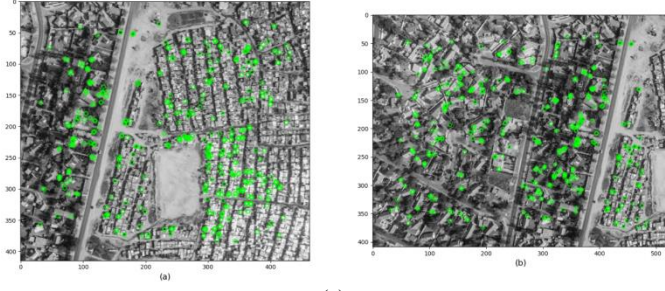
(a)

(b)



(a)

(b)



(a)

(b)

Fig. 5. Features Extracted (a) SIFT (b) BRISK (c) Proposed.



(c)

Fig. 6. Matching features (a) SIFT (b) BRISK (c) Proposed.



Fig. 7. Final stitched image.

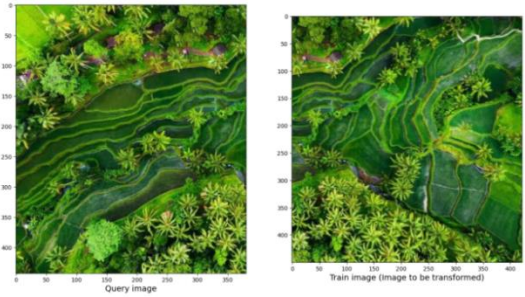
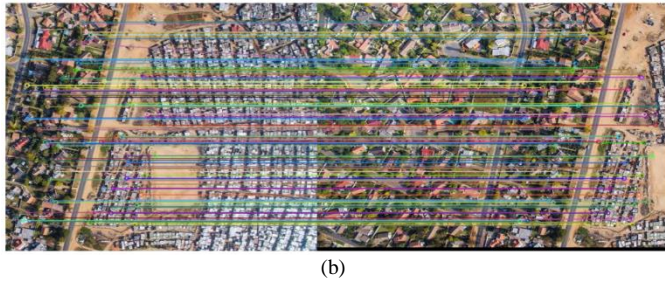


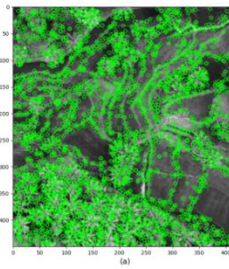
Fig. 8. Input sample 2: image1 and image2.



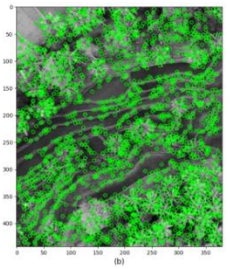
(a)



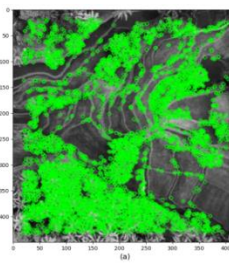
(b)



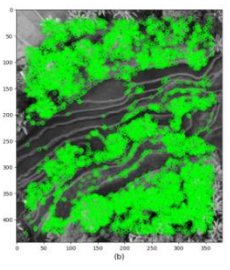
(a)



(b)



(a)



(b)

(a)

(b)

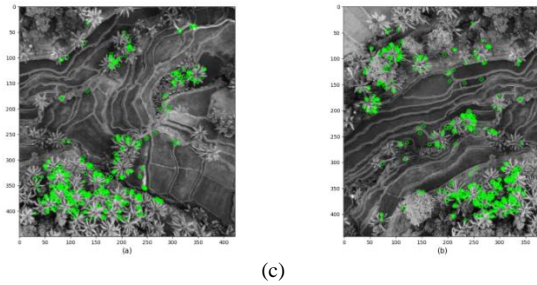


Fig. 9. Features extracted (a) SIFT (b) BRISK (c) Proposed.

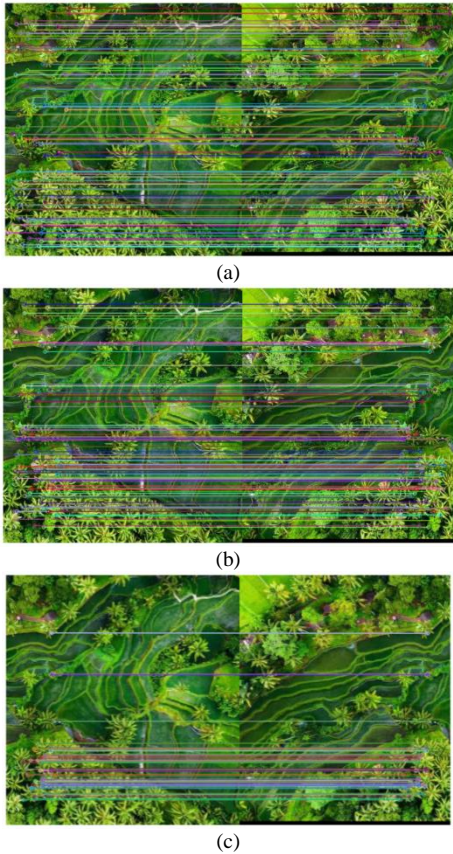


Fig. 10. Matching features (a) SIFT (b) BRISK (c) Proposed.

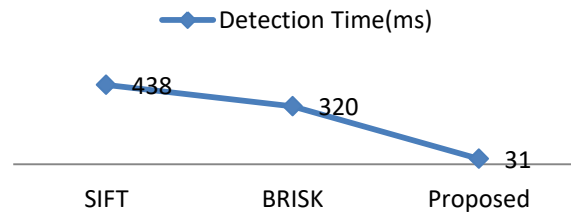


Fig. 11. Final stitched image.

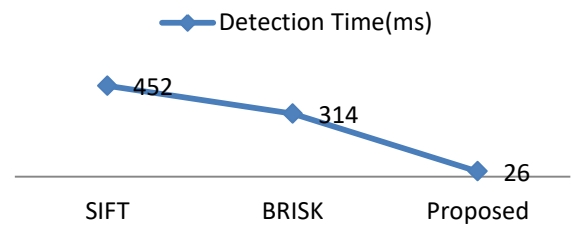
Fig. 8 shows the input sample 2 image pairs to be stitched. During feature extraction using SIFT algorithm, 3532 features from the first image and 2754 features from the second image are selected as shown in Fig. 9(a) using SIFT. Fig. 9(b) shows the 5057 features and 5128 features selected from images 1 and 2, respectively using BRISK algorithm. Fig. 9(c) shows the

475 features from Image 1 and 480 features from image 2 selected using the proposed approach. Fig. 10(a), (b) and (c) shows the matching features between the pairs of images using SIFT, BRISK and the proposed algorithm respectively. Fig. 11 is the stitched image of sample 2 image pairs.

Fig. 12(a) and (b) shows the detection time for feature selection for image mapping for sample 1 image pairs. Fig. 13(a) and (b) shows the detection time for feature selection for image mapping for sample 2 image pairs. The detection time for feature extraction clearly represents that the proposed work is 14 times and ten times faster than the SIFT and BRISK algorithms for the image 1 of sample 1; 17 times and 12 times faster than the SIFT and BRISK algorithms for the image 2 of sample 1; 11 times and nine times faster than the SIFT and BRISK algorithms for the image 1 of sample 2; 9 times and ten times faster than the SIFT and BRISK algorithms for the image 2 of sample 2. Overall, the proposed algorithm on average is 13 times faster than the SIFT algorithm and ten times faster than the BRISK algorithm.

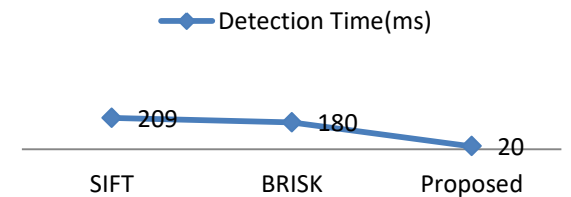


(a)

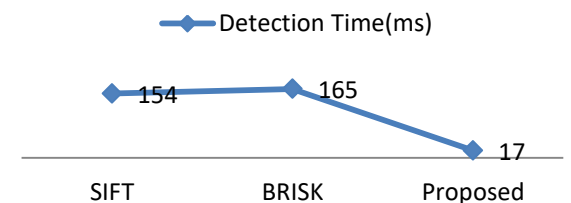


(b)

Fig. 12. Detection times of sample 1 image pairs.



(a)



(b)

Fig. 13. Detection times of sample 2 image pairs.

## VI. CONCLUSION

In this work we have proposed a new technique for image fusion using signal extraction technique behind the brain waves using EEG. Decortification technique is used in processing and preparing the images for matching and blending. Live UAV video frames are fused and can be used for various applications like target tracking and distance measurement. The proposed work is able to choose optimal features with good image understanding. The suggested approach outperforms the SIFT and BRISK algorithms on average by a factor of 13 and 10, respectively. In future the proposed work will be implemented in test-bed for live frame sequence transformations to fused images.

## REFERENCES

- [1] Mhangara, P., Mapurisa, W., & Mudau, N., "Comparison of Image Fusion Techniques Using Satellite Pour P", *Observation de la Terre (SPOT), 6 Satellite Imagery, Applied Sciences*, 2020.
- [2] Jung, H., Kim, Y., Jang, H., Ha, N., & Sohn, K., "Unsupervised Deep Image Fusion With Structure Tensor Representations", *IEEE Transactions on Image Processing*, 29, 3845-3858, 2020.
- [3] Dogra, A., Goyal, B., & Agrawal, S., "Multi-Scale Decomposition to Non-Multi-Scale Decomposition Methods: A Comprehensive Survey of Image Fusion Techniques and Its Applications", *IEEE Access*, 5, 16040-16067, 2017.
- [4] Haskins, G., Kruecker, J., Kruger, U., Xu, S., Pinto, P., Wood, B., & Yan, P., "Learning deep similarity metric for 3D MR-TRUS image registration", *International Journal of Computer Assisted Radiology and Surgery*, 14, 417-425, 2018.
- [5] Yurduseven, O., Fromenteze, T., & Smith, D., "Relaxation of Alignment Errors and Phase Calibration in Computational Frequency-Diverse Imaging using Phase Retrieval", *IEEE Access*, 6, 14884-14894, 2018.
- [6] He, J., Sun, M., Chen, Q., & Zhang, Z., "An improved approach for generating globally consistent seamline networks for aerial image mosaicking", *International Journal of Remote Sensing*, 40, 859 – 882, 2018.
- [7] Zhaoxiang, Z., Iwasaki, A., & Xu, G., "Attitude Jitter Compensation for Remote Sensing Images Using Convolutional Neural Network", *IEEE Geoscience and Remote Sensing Letters*, 16, 1358-1362, 2019.
- [8] Su, Z., Wang, F., Xiao, H., Yu, H., & Dong, S., "A fault diagnosis model based on singular value manifold features, optimized SVMs and multi-sensor information fusion", *Measurement Science and Technology*, 2020.
- [9] Guan, B., Zhao, J., Li, Z., Sun, F., & Fraundorfer, F., "Relative Pose Estimation With a Single Affine Correspondence", *IEEE Transactions on Cybernetics*, 52, 10111-10122, 2021.
- [10] DeTone, Daniel, Tomasz Malisiewicz, and Andrew Rabinovich. "Superpoint: Self-supervised interest point detection and description." *Proceedings of the IEEE conference on computer vision and pattern recognition workshops*. 2018.
- [11] Moniruzzaman, M. D., et al. "Teleoperation methods and enhancement techniques for mobile robots: A comprehensive survey." *Robotics and Autonomous Systems*, 150, 103973, 2022.
- [12] Nie, Lang, et al. "A view-free image stitching network based on global homography." *Journal of Visual Communication and Image Representation* 73,102950, 2020.
- [13] Avola, Danilo, et al. "Automatic estimation of optimal UAV flight parameters for real-time wide areas monitoring." *Multimedia Tools and Applications* 80 (2021): 25009-25031.
- [14] Li, Ronghao, et al. "A Real-Time Incremental Video Mosaic Framework for UAV Remote Sensing." *Remote Sensing* 15.8, 2127, 2023.
- [15] Srivastava, Srishiti, Sarthak Narayan, and Sparsh Mittal. "A survey of deep learning techniques for vehicle detection from UAV images." *Journal of Systems Architecture* 117 (2021): 102152.
- [16] Woo, Hyun-Jung, et al. "Localization of Cracks in Concrete Structures Using an Unmanned Aerial Vehicle", *Sensors* 22.17, 6711, 2022.
- [17] Rui, Ting, et al. "Research on fast natural aerial image mosaic", *Computers & Electrical Engineering*, 90107007, 2021.
- [18] Zhang, Gengxin, et al. "UAV low-altitude aerial image stitching based on semantic segmentation and ORB algorithm for urban traffic." *Remote Sensing* 14.23, 6013, 2022.
- [19] Yuan, Yiting, Faming Fang, and Guixu Zhang. "Superpixel-based seamless image stitching for UAV images." *IEEE transactions on geoscience and remote sensing* 59.2 (2020): 1565-1576, 2020.
- [20] Yang, Cong, et al. "Towards accurate image stitching for drone-based wind turbine blade inspection." *Renewable Energy* 203 (2023): 267-279.
- [21] Do, Hai T., et al. "Energy-efficient unmanned aerial vehicle (UAV) surveillance utilizing artificial intelligence (AI)." *Wireless Communications and Mobile Computing*, pp 1-11, 2021.
- [22] Subha, D.P., Joseph, P.K., Acharya U, R. et al., *EEG Signal Analysis: A Survey*. *J Med Syst* 34, 195–212, 2010.
- [23] Singh, Kuldeep, Sukhjeet Singh, and Jyoteesh Malhotra. "Spectral features based convolutional neural network for accurate and prompt identification of schizophrenic patients." *Proceedings of the Institution of Mechanical Engineers, Part H: Journal of Engineering in Medicine* 235.2, 167-184, 2021.
- [24] Wen, Tee Yi, and SA Mohd Aris. "Electroencephalogram (EEG) stress analysis on alpha/beta ratio and theta/beta ratio." *Indones. J. Electr. Eng. Comput. Sci* 17.1, 175-182, 2020.
- [25] A. Annis Fathima, R. Karthik, V. Vaidehi, *Image Stitching with Combined Moment Invariants and Sift Features*, *Procedia Computer Science*, Volume 19, Pages 420-427, ISSN 1877-0509, 2013.
- [26] Yanli Liu, Heng Zhang, Hanlei Guo and Neal N. Xiong. "A FAST-BRISK Feature Detector with Depth Information", *Sensors (Basel)*, Nov 18(11): 3908, 2018.